Light deflection by light: Effect of incidence angle and inhomogeneity

Pardeep Kumar* and Shubhrangshu Dasgupta
Department of Physics, Indian Institute of Technology Ropar, Rupnagar, Punjab 140001, India
(Received 16 March 2016; published 24 October 2016)

We study the angular deflection of the circularly polarized components of a linearly polarized probe field in a weakly birefringent atomic system in tripod configuration. A spatially inhomogeneous control field incident obliquely onto an atomic vapor cell facilitates a large angular divergence between circular components. We show that the angular resolution can be dynamically controlled by optimally choosing the angle of incidence and the transverse profile of the control beam. For instance, by employing a Laguerre-Gaussian profile of the control field, one can impart a large angular divergence to the circular components close to the entry face of the atomic vapor cell. We further demonstrate how such a medium causes the focusing and refocusing of the probe field, thereby acting as a lens with multiple foci. The absorption in the medium remains negligible at resonance due to electromagnetically induced transparency.

DOI: 10.1103/PhysRevA.94.043845

I. INTRODUCTION

Many optical phenomena such as refraction and dispersion involve a change in the trajectory of the incident light as a consequence of the spatial variation of the refractive index of the medium. In the past decades, optical beam deflection has achieved considerable attention. The deflection of light beam can be achieved by mechanical interaction [1], thermal gradient [2], acousto-optical interaction [3], electro-optic effect [4], and all-optical methods [5]. Optical methods have enjoyed much attention due to their high speed, efficiency, and fast nonlinear response time.

Maneuvering light by another light through their interaction with the medium has thus created a new avenue of research. Much interest has been given to the deflection of light beam in a homogeneous medium subjected to external fields with spatially inhomogeneous intensity distributions. The spatial modulation of the refractive index of the medium induced by a suitable inhomogeneous control field leads to several effects, such as dynamic light deflection [6,7], waveguiding [8], and antiwaveguiding [9]. A significant variation of the refractive index at resonance can give rise to large deflection. Recently, such a deflection in an atomic medium, exhibiting electromagnetically induced transparency (EIT), has been observed in the presence of a *magnetic field* with small gradient transverse to the propagation direction [10–12]. In another related experiment [13], it was found that the light ray can also be deflected when an *optical field* with inhomogeneous transverse profile drives a cell with Rb atomic vapors with an Λ-type energy-level configuration. The angle of deviation obtained by means of an optical field is found to be much larger (by several orders) than that reported using an inhomogeneous magnetic field [12]. An adequate explanation for the observed phenomenon of light deflection can be provided in the framework of semiclassical theory [14,15]. Further, the beam deflection in an EIT medium can also be explained quantum mechanically in terms of a dark state *polariton* possessing an effective magnetic moment [12,16,17]. Besides this, the deflection of light in terms of *vector optical solitons* (nonlinear polariton) in a double EIT system is proposed in Ref. [18]. Further, in comparison to an EIT medium, an active Raman gain (ARG) medium is shown to induce larger deflection of light beams [19] and antiwaveguiding [20].

In order to measure the small deflections of beams, many sophisticated interferometric setups have been proposed [21,22]. Some of these techniques are inspired by quantum *weak measurement* [23] to resolve angstrom-scale optical beam deflection in space as well as in time domain [24,25]. In this paper, instead of making sensitive detection of small deflection, we rather propose a way to increase the angular separation between the circular components of the probe field by using an inhomogeneous control field in an atomic vapor system with tripod configuration. We present a theoretical analysis (in the framework of *semiclassical* theory) to demonstrate light deflection where the control beam is incident obliquely to the entrance face of the vapor cell. This oblique incidence of the control beam causes the mixing of the excitations on all three optical transitions in the tripod system, leading to an extra flexibility to produce large angular divergence among $\sigma_{\pm}$ components of the probe field by changing the angle of incidence. It should be borne in mind that a medium of chiral molecules also creates the birefringence and hence the angular divergence between the circular components of the linearly polarized light. In Ref. [26], it has been demonstrated that such an effect can occur at the interface of achiral and chiral media and can be used for the detection of optical activity [27] with a *miniaturized* sample volume. Here, we mimic such a situation in *atomic vapors* by exploiting large angular divergence *close to the entry face* of the vapor cell.

Note that an inhomogeneous control field can create a birefringence inside a medium [28]. By suitably choosing the transverse profile of the control field, one can enhance this birefringence to impart larger angular divergence to the orthogonal components. We show that by choosing a Laguerre-Gaussian profile [29] of the control field, angular divergence can be made larger, compared to that obtained using a Gaussian profile. This also results in the focusing and refocusing effects of $\sigma_{\pm}$ components of the probe field at various axial positions. We detect a few focal points for the probe field depending on the profile and the incidence angle of the control beam. Thereby, a medium with suitable length

*pradeep.kumar@iitrpr.ac.in

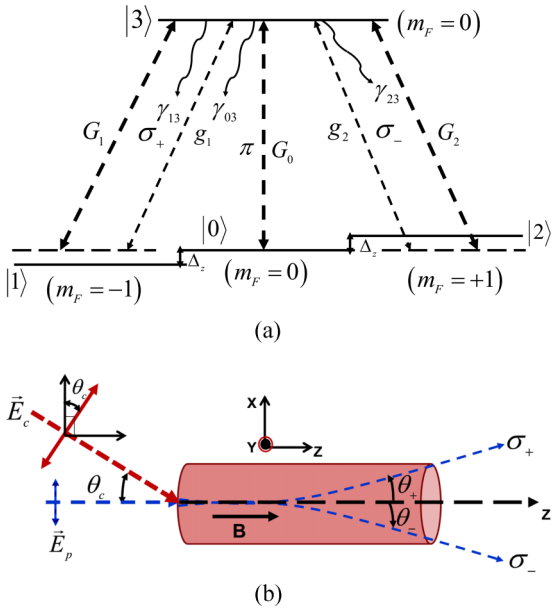

FIG. 1. (a) Energy-level configuration. The $\sigma_\pm$ components of the probe field drive the transitions $|1\rangle \leftrightarrow |3\rangle$ and $|2\rangle \leftrightarrow |3\rangle$, respectively. A control field incident at an angle θ_c to the entry face excites all the transitions of the tripod system. The degeneracy of the ground levels is removed by applying a feeble axial magnetic field. γ_{j3} $(j = 0,1,2)$ are the spontaneous decay rates from $|3\rangle$ to $|j\rangle$. (b) Schematic for the deflection of the circular components of the probe field.

behaves as a lens [16] with multiple foci. It is to be emphasized that the large angular divergence of the circular components of the probe field is accompanied by zero absorption at resonance, thanks to EIT [30]. This suggests a way to obtain sufficiently large deflection, even with an EIT medium, instead of an ARG medium.

The organization of the paper is as follows. In Sec. II, the theoretical model is introduced along with the eikonal approximation for the probe deflection. The influence of the angle of incidence and the profile of the control field on the deflection and the transmission of circular components of the probe field is described in Sec. III. In this section, the main results of the paper are presented. Section IV summarizes this paper.

II. PHYSICAL MODEL

We consider a generic four-level tripod atomic system, as shown in Fig. 1(a). The relevant energy levels can be found in many systems, such as in ^{39}K [31], ^{23}Na [32], ^{7}Li [33], and Pr:YSO [34]. Here, we used the transition $^2S_{1/2} \rightarrow {}^2P_{1/2}$ at 769.9 nm of ^{39}K vapors. The ground levels are $|1\rangle = {}^2S_{1/2}(F = 2, m_F = -1)$, $|0\rangle = {}^2S_{1/2}(F = 2, m_F = 0)$, and $|2\rangle = {}^2S_{1/2}(F = 2, m_F = +1)$, and the upper state is $|3\rangle = {}^2P_{1/2}(F = 1, m_F = 0)$. The upper level $|3\rangle(m_F = 0)$ is coupled to the ground levels $|1\rangle(m_F = +1)$ and $|2\rangle(m_F = -1)$ by a $\hat{x}$-polarized weak probe field $\vec{E}_p = \hat{x}\varepsilon_p e^{-i(\omega_p t - k_p z)} + \text{c.c.}$ propagating along the z direction. Here, ε_p is the slowly varying envelope, ω_p is the angular frequency, and k_p is the propagation constant of the probe field. The orthogonal components of the probe with σ_+ and σ_- polarizations couple to $|1\rangle \leftrightarrow |3\rangle$ and $|2\rangle \leftrightarrow |3\rangle$ transitions, respectively. The Rabi frequencies of the corresponding transitions are defined as $2g_1 = 2(\frac{\vec{d}_{31}\cdot\hat{x}\varepsilon_p}{\hbar})$ and $2g_2 = 2(\frac{\vec{d}_{32}\cdot\hat{x}\varepsilon_p}{\hbar})$, where $\vec{d}_{ij}$ represents the transition electric dipole moment matrix element between the levels $|i\rangle$ and $|j\rangle$. The degeneracy of the ground level has been removed by applying a dc magnetic field of strength B along the quantization z axis. The Zeeman splitting among the respective levels is $\Delta_z = \mu_B B m g_F/h$, where μ_B is Bohr magneton and g_F is the hyperfine Landé g factor. A control field $\vec{E}_c = \varepsilon_c(\cos\theta_c\hat{x} + \sin\theta_c\hat{z})e^{ik_c(-x\sin\theta_c + z\cos\theta_c) - i\omega_c t} + \text{c.c.}$ is incident obliquely at an angle θ_c to the medium with polarization lying in the plane of incidence, as shown in Fig. 1(b). Here, ε_c, k_c, and ω_c are the slowly varying envelope, propagation constant, and frequency of the control field. This field couples to $|j\rangle \leftrightarrow |3\rangle$ $(j = 0,1,2)$ transitions. The corresponding Rabi frequencies of the control field are given by $2G_i = 2[\varepsilon_c(\cos\theta_c\hat{x} + \sin\theta_c\hat{z})]\cdot\vec{d}_{ji}/\hbar$ $(i = 0,1,2$ and $j = 3)$. Using the circular polarization vector $\hat{\epsilon} = (\hat{x} \pm i\hat{y})/\sqrt{2}$, these Rabi frequencies can be simplified as

$$G_1 = \frac{|\vec{d}|\varepsilon_c}{\hbar\sqrt{2}}\cos\theta_c, \quad G_2 = \frac{|\vec{d}|\varepsilon_c}{\hbar\sqrt{2}}\cos\theta_c, \quad G_0 = \frac{|\vec{d}_{30}|\varepsilon_c}{\hbar}\sin\theta_c, \tag{1}$$

where the dipole matrix element $(\vec{d}_{ji})$ is written using Clebsch-Gordan coefficients as $|\vec{d}_{31}| = |\vec{d}_{32}| = |\vec{d}|$ and $|\vec{d}_{30}| = \sqrt{\frac{4}{3}}|\vec{d}|$.

The Hamiltonian for the above system in dipole approximation can be written as

$$\hat{H} = \sum_{j=1}^{3}\hbar\omega_{j0}|j\rangle\langle j| - \sum_{k=0}^{2}(G_k e^{-i\omega_c t}|3\rangle\langle k| + \text{H.c.}) - \sum_{k=1}^{2}(g_k e^{-i\omega_p t}|3\rangle\langle k| + \text{H.c.}). \tag{2}$$

Here, zero of energy is defined at the level $|0\rangle$ and $\hbar\omega_{\alpha\beta}$ is the energy difference between the levels $|\alpha\rangle$ and $|\beta\rangle$. We describe the dynamical evolution of the system by the density matrix equations in the Markovian limit, as given in the Appendix.

A. Susceptibility of the atomic medium

In the steady state, we can obtain the approximate solution for the linear susceptibility of the medium for the probe field. Here, we are interested in the atomic coherences $\tilde{\rho}_{31}^{(+1)}$ and $\tilde{\rho}_{32}^{(-1)}$ for the orthogonal components of the probe field, which can be obtained by solving Eq. (A3). Thus, the susceptibility of the atomic medium for the orthogonal components of the probe field is given by

$$\chi_+ = \frac{3Nc^3}{2\omega_p^3}\tilde{\rho}_{31}^{\prime(+1)}, \quad \chi_- = \frac{3Nc^3}{2\omega_p^3}\tilde{\rho}_{32}^{\prime(-1)}, \tag{3}$$

where N is the number density of the atomic medium and c is the speed of light in vacuum.

B. Probe deflection

In general, the spatial structure of the applied fields results in the position dependence of the medium susceptibility

[Eq. (3)]. The trajectory of a light ray propagating through an inhomogeneous medium can be found by solving an eikonal equation [35],

$$(\nabla\psi)\cdot(\nabla\psi) = n^2, \tag{4}$$

where the eikonal ψ represents the phase of the electromagnetic wave and $n = 1 + 2\pi\mathrm{Re}[\chi]$ describes the refractive index of the medium. Now, by defining $\nabla\psi = n\frac{d\vec{R}}{ds}$, we obtain the following differential equation:

$$\frac{d}{ds}\left(n\frac{d\vec{R}}{ds}\right) = \nabla n. \tag{5}$$

Here, $\vec{R} = X(z)\hat{e}_x + Y(z)\hat{e}_y + z\hat{e}_z$ is a point on the light ray and $ds = \sqrt{dx^2 + dy^2 + dz^2}$. In component form, Eq. (5) yields

$$\frac{d}{ds}\left(n\frac{dX}{ds}\right) = \frac{\partial n}{\partial x}, \quad \frac{d}{ds}\left(n\frac{dY}{ds}\right) = \frac{\partial n}{\partial y}, \quad \frac{d}{ds}\left(n\frac{dz}{ds}\right) = \frac{\partial n}{\partial z}. \tag{6}$$

In the paraxial limit, $ds \approx dz$ for small deflections and the first two equations in Eq. (6) reduce to an ordinary differential equation describing the ray trajectories, as follows:

$$\frac{d^2X}{dz^2} = \frac{\partial n}{\partial x} \quad \text{and} \quad \frac{d^2Y}{dz^2} = \frac{\partial n}{\partial y}. \tag{7}$$

Using Eq. (7), the trajectory of the ray and the deflection angle can be estimated. Let us assume that the atomic vapor cell can be divided into many smaller cells such that the external inhomogeneous field appears to be homogeneous for each smaller cell. Thus, the angle of deflection for the probe field [13] can be obtained from Eq. (7) by solving

$$\frac{d\tan\theta_x}{dz} = \frac{\partial n}{\partial x} \quad \text{and} \quad \frac{d\tan\theta_y}{dz} = \frac{\partial n}{\partial y}, \tag{8}$$

where $\tan\theta_x = \frac{dX}{dz}$ ($\tan\theta_y = \frac{dY}{dz}$) represents the slope and θ_x (θ_y) is the angle of deflection of the light rays in the xz plane (yz plane). For smaller angle of deflection, $\tan\theta_x \approx \theta_x$ ($\tan\theta_y \approx \theta_y$), and Eq. (8) yields

$$\theta_x = \int_0^L dz\frac{\partial n}{\partial x} \quad \text{and} \quad \theta_y = \int_0^L dz\frac{\partial n}{\partial y}, \tag{9}$$

where L is the length of the medium in the direction of propagation. In this paper, we consider that the transverse profile of the control field is confined to the $y = 0$ plane. Due to the anisotropy induced by the magnetic field and the inhomogeneous control field [28], the refractive index $n_\pm$ and the corresponding angle of deflection $\theta_\pm$ of the $\sigma_\pm$ components will be different, giving rise to an *angular divergence* $\phi = \theta_+ - \theta_-$.

C. Transmission of circular components

Further, the imaginary part of the susceptibilities $\chi_\pm$ [Eq. (3)] determines the transmission of the right and left circularly polarized components of the probe field. These susceptibilities depend upon the transverse profile of the control field, and therefore the transmission of the circular components can be written as

$$T_\pm(x,y,L) = \exp\left\{-k_p\int_0^L \mathrm{Im}[\chi_\pm(x,y,z;\omega_p)]dz\right\}, \tag{10}$$

which under the paraxial approximation reduces to

$$T_\pm(L) = \exp\left\{-k_p\int_0^L \mathrm{Im}[\chi_\pm(z;\omega_p)]dz\right\}. \tag{11}$$

III. RESULTS

A. Beam profile of the control field

In order to produce the spatially dependent refractive index for the probe field, we choose the following transverse profile of the control field:

$$\varepsilon_c(x,y,z) = \varepsilon_0\frac{w_0}{w_z}\left(\frac{\sqrt{2}r}{w_z}\right)^m e^{-\frac{r^2}{w_z^2}}\exp\left[-\frac{ikr^2}{2R_z} + im\theta\right] \times \exp\left[-i(m+1)\tan^{-1}\left(\frac{Z}{z_R}\right)\right], \tag{12}$$

where ε_0 is the initial peak amplitude, $w_z = w_0\sqrt{1 + (Z/z_R)^2}$ is the beam width with w_0 as the beam waist at $Z = 0$, and $z_R = \pi w_0^2/\lambda$ is the Rayleigh length. Here, $r = \sqrt{X^2 + y^2}$ is the radial distance from the axis of the beam, $\theta = \tan^{-1}(\frac{y}{X})$ and $R_z = Z[1 + (\frac{z_R}{Z})^2]$. As the control field is incident at an angle θ_c to the vapor cell, we can write $X = x\cos\theta_c - z\sin\theta_c$ and $Z = x\sin\theta_c + z\cos\theta_c$ as the coordinates in the plane of incidence. For $m = 0$, the above profile becomes Gaussian, and takes the following simplified form:

$$\varepsilon_c(x,y,z) = \varepsilon_0'\exp\left(-\frac{X^2 + y^2}{\sigma^2}\right), \tag{13}$$

where ε_0' defines the maximum amplitude of the Gaussian beam and σ refers to its transverse width. Note that the full width at half maxima (FWHM) of the above profile is $2\sqrt{2\ln 2}\sigma$.

On the other hand, $m \neq 0$ corresponds to a Laguerre-Gaussian $(\mathrm{LG})_m$ profile with azimuthal index m. Such a spatial structure of the control field produces inhomogeneity for the susceptibility of the probe field along the transverse direction and results in its deflection.

B. Dependence of angular divergence on angle of incidence

To delineate the effect of angle of incidence on the angular divergence between $\sigma_\pm$ components of the probe field, we first consider a Gaussian profile (LG_0) of the control field. At two-photon resonance, this profile creates transparency for the probe field at $x = 0$, whereas the position-dependent refractive index remains zero. The circular components of the probe field experience deflection if the probe is off-centered with respect to the control field. We demonstrate in Fig. 2 the variation of the angular divergence between the orthogonal polarized components of the probe field along with the respective transparencies with the longitudinal distance L for different values of the angle of incidence at $y = 0$ plane. The angular divergence has a dispersionlike profile with maxima and minima at different axial positions, as shown in Fig. 2. Note that the deflection

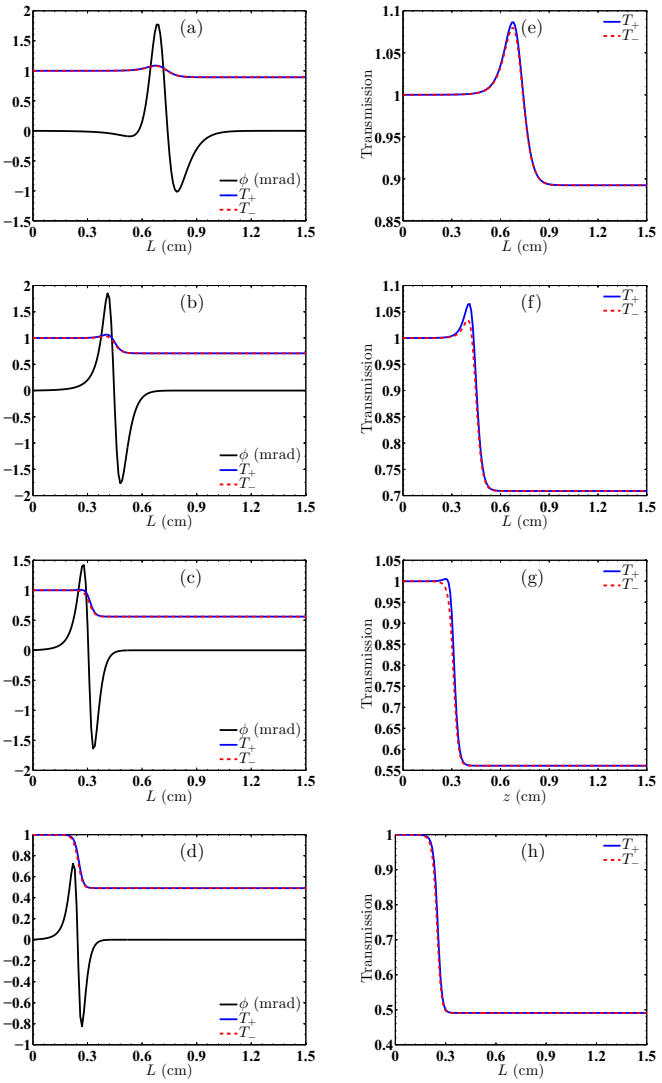

FIG. 2. Variation of angular divergence (ϕ) (solid black line) between the circular components and the respective transmission of the circular components (solid blue line for σ_+ and dashed red line for σ_-) with the propagation distance L (cm) for a Gaussian profile of the control field with (a) $\theta_c = \pi/10$, (b) $\theta_c = \pi/6$, (c) $\theta_c = \pi/4$, and (d) $\theta_c = \pi/3$. The corresponding transmission is also shown in the inflated graphs (e)–(h) for the respective θ_c's. We have used the parameters for ^{39}K vapor with $A = 2\pi \times 6.079$ MHz, $\gamma = \frac{A}{12}$, $\lambda = 769.9$ nm, and $N = 5 \times 10^{12}$ cm^{-3}. Other parameters are $\Delta_z = 0.01\gamma$ (32 kHz), $\delta = 0$, $\Delta = 0$, $\gamma_{13} = \gamma_{23} = \gamma_{03} = \gamma$, and $\gamma_{\text{coll}} = 0$, and the transverse width (σ) of the Gaussian profile is taken to be $\sqrt{2}$ mm.

of $\sigma_\pm$ components occurs within a short distance from the interface. The maxima and minima of the angular divergence occur at a larger distance for smaller angle of incidence. For smaller angle of incidence, the inhomogeneous control field moves close to the axis of the probe field in the vapor cell and a larger overlap area of these fields causes the angular divergence to happen at longer propagation distance [see Fig. 2(a)]. It is to be emphasized that during the deflection, the circular components of the probe field remain transparent for the positive deflection, thanks to EIT. But, for negative deflection, these components suffer absorption for the Gaussian profile of the control field, as shown in Figs. 2(e)–2(h). Moreover, the absorption dominates in the system for the negative deflection as the angle of incidence of the control field increases [see Fig. 2(h)]. Furthermore, for larger angle of incidence [say $\theta_c = \pi/4$; Fig. 2(c)], the maximum deflection happens to be at distance $L \approx$ FWHM of the control field. Thus, the angle of incidence of the control field provides a flexibility to the control of the angular divergence of the polarized components of the probe field.

It is to be noted that a reasonable explanation for such a light deflection can be given in terms of the spatially dependent potential induced by the coupling between the atoms and the light [17]. The transverse profile of the control field decides the shape of such a potential. Thus, a probe field of width smaller than the width of the control field gets deflected if it is adjusted to the left or to the right side of the control field. Further, the deflection of the light in an EIT medium can also be described quantum mechanically with the dark state *polariton* possessing an effective magnetic moment [12,16,17].

C. Effect of the profile of the control field

In the preceding analysis, we have discussed how the Gaussian profile of the control field causes the deflection of the circularly polarized components of the probe field. Next, we discuss the effect of the profile of the control beam on the angular divergence between $\sigma_\pm$ components together with the substantial improvement of the transmission of the probe field. For this purpose, we consider a doughnut-shaped Laguerre-Gaussian mode (LG_3) for the control beam. In Fig. 3, we exhibit the dependence of the angular divergence and the transmission of circular components on the propagation distance for different values of the incident angles of the control field. Clearly, a comparison of Figs. 2 and 3 reveals that the doughnut-shaped LG_3 mode is better than the Gaussian mode to produce larger angular divergence. Also, for LG_3 transverse profile of the control field, $\sigma_\pm$ components of the probe field remain nearly transparent throughout their propagation, as depicted in Figs. 3(e)–3(h). More interestingly, for the Laguerre-Gaussian mode, the large deflection occurs without much absorption within a very short distance from the entrance face of the vapor cell. This feature mimics the refraction of a linearly polarized light from the interface, as in the case of a medium with chiral molecules [26]. For a medium having natural anisotropy due to the presence of chiral molecules, a linearly polarized incident light splits into circularly polarized components just at the interface. Here, we have shown such an effect in a simple atomic system. Furthermore, the location of maximum angular divergence of the orthogonal components close to the entry face of the atomic vapor cell can be modified by changing the beam waist. Increase in the beam waist causes the deflection to happen at longer distance.

D. Lens effects of a coherently prepared atomic medium

The above analysis implies the deflection of the orthogonally polarized components of the probe field through a coherently prepared medium. Now, we demonstrate that such

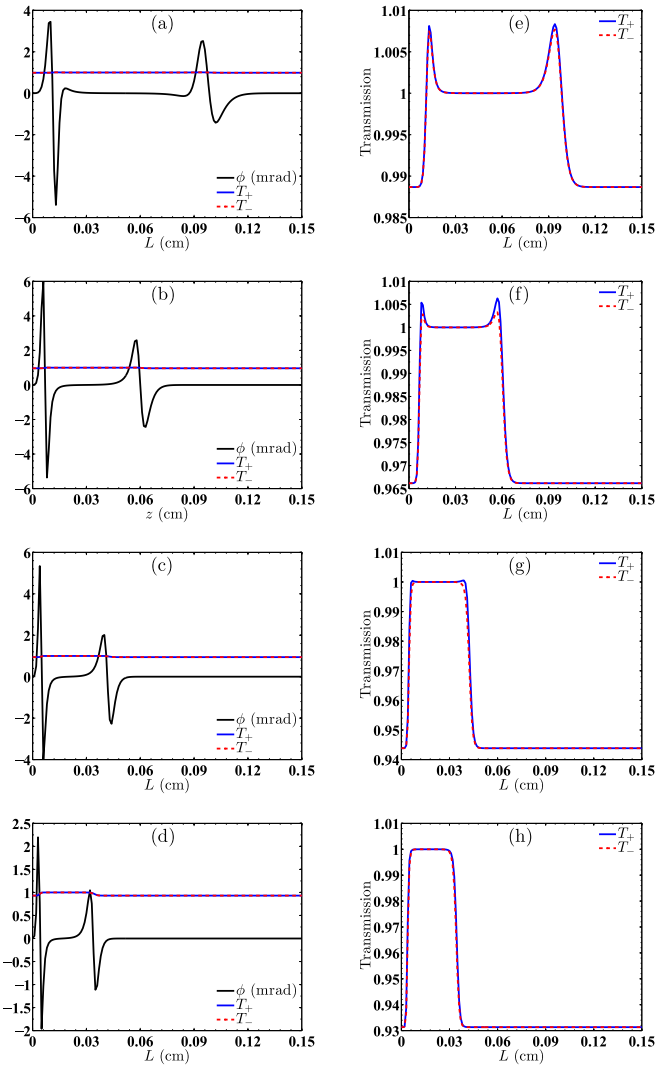

FIG. 3. Variation of angular divergence (ϕ) (solid black line) between the circular components of the probe field and the respective transmission of the circular components (solid blue line for σ_+ and dashed red line for σ_-) with the propagation distance L (cm) for a Laguerre-Gaussian profile (with $m = 3$) of the control field with (a) $\theta_c = \pi/10$, (b) $\theta_c = \pi/6$, (c) $\theta_c = \pi/4$, and (d) $\theta_c = \pi/3$. The corresponding transmission is also shown in the inflated graphs (e)–(h) for the respective θ_c's. The parameters used are beam waist $(w_0) = 120$ μm, Rayleigh length $(z_R) = 5.7$ cm, and the other parameters are the same as in Fig. 2.

a medium behaves as a lens with a varying focus which can be controlled optically. Such a lens causes the focusing and refocusing of $\sigma_\pm$ components. This is demonstrated in Fig. 4. For the Gaussian profile of the control beam [Fig. 4(a)], the two orthogonal circular components converge at a point f_1 which refers to a focal point. On the other hand, for an LG_3 transverse profile of the control field [Fig. 4(b)], $\sigma_\pm$ components refocus at f_2 after focusing at f_1, thereby producing two focal points. Thus, a coherent medium behaves as a converging lens, the number of focal points of which can be controlled optically. Further, the location of the focal points can be varied by changing the angle of incidence of the control field. Thus, the profile of the control beam and its angle of incidence act as

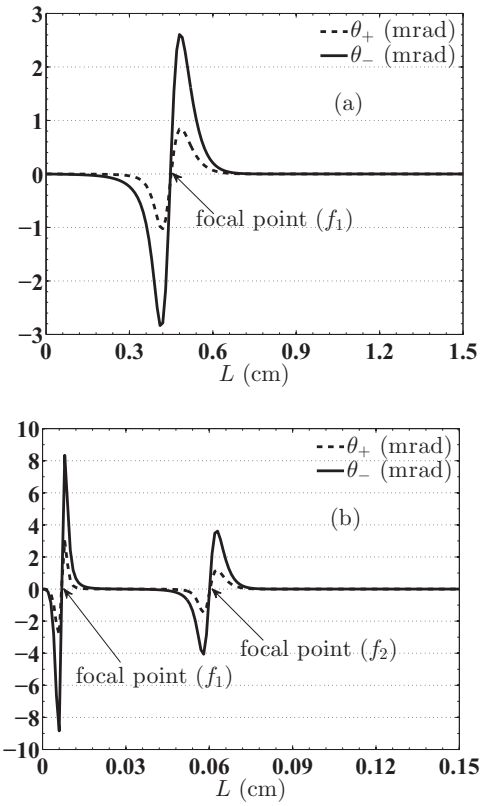

FIG. 4. The deflection of $\sigma_\pm$ components of the probe field with the propagation length L (cm) for (a) the Gaussian and (b) the LG_3 profile of the control field. We have chosen $\theta_c = \pi/6$ and the rest of the parameters are the same as in Fig. 2.

a knob to control the focusing and refocusing of the probe field while passing through an optically controlled atomic medium.

IV. CONCLUSIONS

In conclusion, we have explored the enhancement of the angular divergence between the orthogonally polarized components of the linearly polarized probe field by using angle of incidence and the profile of the control beam as a knob. Such an effect can be enhanced by using higher-order Laguerre-Gaussian modes in the profile of the control field. For the LG_3 mode, the maximum deflection happens close to the entry face of the vapor cell. Moreover, a large angular divergence close to the entry face is accompanied by negligible absorption due to EIT. We further show how the coherent atomic medium can act as a lens with multiple foci, depending upon the profile and the angle of incidence of the control beam. However, the large value of angular divergence of the circular components of the probe field is limited by broadening mechanisms, viz., Doppler broadening and collisional broadening. These mechanisms result in the decrease of the angular deflection between the circular components of the probe field. For instance, at $\theta_c = \pi/6$, the maximum angular divergence for an LG_3 (Gaussian) profile of the control is figured to be 0.2 mrad (0.05 mrad) for $\gamma_{\rm coll} = 0.1\gamma$.

Besides this, the present scheme holds promise to spatially resolve the circular components of a linearly polarized probe

field just by changing the angle of incidence of the inhomogeneous control field. Thus, such a medium can be used as a polarization splitter towards the spatially distinguishable channels for polarization. Additionally, the use of angle of incidence as a knob to enhance the angular divergence provides an extra flexibility over other parameters such as detuning [13]. Further, the large angular divergence close to the entry face of the atomic vapor cell is analogous to the angular divergence of the circular components of the probe field on the interface of achiral-chiral media, leading to the miniaturization of the sample volume [26]. As another application, such a medium can be used as an atomic lens, thereby causing the focusing and refocusing effects of the probe light [16]. Moreover, the spatial modulation of the refractive index in such an EIT medium finds applications in optical steering [14], all-optical delay lines for radar systems [36], high spectral resolution spectrometer [13], waveguiding [37], and antiwaveguiding [9].

APPENDIX: RELEVANT DENSITY MATRIX EQUATIONS

To describe the dynamics of the system, we use the Markovian master equation under rotating-wave approximation by including the natural decay terms, and the following density matrix equations are obtained:

$$
\begin{aligned}
\dot{\tilde{\rho}}_{11} &= \gamma_{13}\tilde{\rho}_{33} - i(g_1 e^{-i\omega_{pc}t}\tilde{\rho}_{13} - \text{c.c.}) - i(G_1\tilde{\rho}_{13} - \text{c.c.}),\\
\dot{\tilde{\rho}}_{22} &= \gamma_{23}\tilde{\rho}_{33} - i(g_2 e^{-i\omega_{pc}t}\tilde{\rho}_{23} - \text{c.c.}) - i(G_2\tilde{\rho}_{23} - \text{c.c.}),\\
\dot{\tilde{\rho}}_{00} &= \gamma_{03}\tilde{\rho}_{33} - i(G_0\tilde{\rho}_{03} - \text{c.c.}),\\
\dot{\tilde{\rho}}_{31} &= [i(\Delta+\Delta_z) - \Gamma_{31}]\tilde{\rho}_{31} + iG_2\tilde{\rho}_{21} + iG_0\tilde{\rho}_{01}\\
&\quad + ig_2 e^{-i\omega_{pc}t}\tilde{\rho}_{21} + i[g_1 e^{-i\omega_{pc}t} + G_1](\tilde{\rho}_{11} - \tilde{\rho}_{33}),\\
\dot{\tilde{\rho}}_{32} &= [i(\Delta-\Delta_z) - \Gamma_{32}]\tilde{\rho}_{32} + ig_1 e^{-i\omega_{pc}t}\tilde{\rho}_{12} + iG_0\tilde{\rho}_{02}\\
&\quad + iG_1\tilde{\rho}_{12} + i[g_2 e^{-i\omega_{pc}t} + G_2](\tilde{\rho}_{22} - \tilde{\rho}_{33}),\\
\dot{\tilde{\rho}}_{30} &= [i\Delta - \Gamma_{30}]\tilde{\rho}_{30} + ie^{-i\omega_{pc}t}(g_1\tilde{\rho}_{10} + g_2\tilde{\rho}_{20})\\
&\quad + i(G_1\tilde{\rho}_{10} + G_2\tilde{\rho}_{20}) + iG_0(\tilde{\rho}_{00} - \tilde{\rho}_{33}),\\
\dot{\tilde{\rho}}_{01} &= [i\Delta_z - \Gamma_{01}]\tilde{\rho}_{01} + iG_0^*\tilde{\rho}_{31} - i[g_1 e^{-i\omega_{pc}t} + G_1^*]\tilde{\rho}_{03},\\
\dot{\tilde{\rho}}_{20} &= -[i\Delta_z + \Gamma_{20}]\tilde{\rho}_{20} - iG_0^*\tilde{\rho}_{23} + i[g_2^* e^{i\omega_{pc}t} + G_2^*]\tilde{\rho}_{30},\\
\dot{\tilde{\rho}}_{21} &= -[2i\Delta_z + \Gamma_{21}]\tilde{\rho}_{21} - i[g_1 e^{-i\omega_{pc}t} + G_1^*]\tilde{\rho}_{23}\\
&\quad + i[g_2^* e^{i\omega_{pc}t} + G_2^*]\tilde{\rho}_{31}.
\end{aligned}
\tag{A1}
$$

The above density matrix equations are subjected to the conditions $\sum_i \tilde{\rho}_{ii} = 1$ and $\tilde{\rho}_{ij} = \tilde{\rho}_{ji}^*$. Here, $\Delta = \omega_c - \omega_{30}(\delta = \omega_p - \omega_{30})$ is the detuning of the control field (probe field) from the $|0\rangle \leftrightarrow |3\rangle$ transition and $\omega_{pc} = \delta - \Delta$ is the frequency difference between probe and control field. Here, γ_{ij} is the spontaneous-emission rate from the level $|j\rangle$ to $|i\rangle$, $\Gamma_{ij} = \gamma_{\text{coll}} + \frac{1}{2}\sum_k(\gamma_{ki} + \gamma_{kj})$ is the dephasing rate of the coherence between the levels $|j\rangle$ and $|i\rangle$, and γ_{coll} is the collisional decay rate. The transformations for the density matrix elements are as follows: $\rho_{3j} = \tilde{\rho}_{3j}e^{-i\omega_c t}(j = 0,1,2)$, and the rest of the elements remain the same. In the weak probe field limit, the density matrix elements can be expanded to first order in g's in terms of the harmonics ω_{pc} as

$$
\begin{aligned}
\tilde{\rho}_{\alpha\beta} &= \tilde{\rho}_{\alpha\beta}^{(0)} + g_1 e^{-i\omega_{pc}t}\tilde{\rho}_{\alpha\beta}^{\prime(+1)} + g_1^* e^{i\omega_{pc}t}\tilde{\rho}_{\alpha\beta}^{\prime\prime(+1)}\\
&\quad + g_2 e^{-i\omega_{pc}t}\tilde{\rho}_{\alpha\beta}^{\prime(-1)} + g_2^* e^{i\omega_{pc}t}\tilde{\rho}_{\alpha\beta}^{\prime\prime(-1)},
\end{aligned}
\tag{A2}
$$

where $\tilde{\rho}_{\alpha\beta}^{(0)}$ represents the zeroth-order solution in the absence of the probe field and $\tilde{\rho}_{\alpha\beta}^{(n)}$ describes the nth-order solution. By substituting Eq. (A2) in Eq. (A1) and equating the like terms, we obtain the following algebraic equations for the zeroth- and first-order coherences:

$$
A_k X_k = B_k \quad (k = 0,\pm). \tag{A3}
$$

The explicit form of the various terms in Eq. (A3) can be written as follows:

$$
A_0 = \begin{bmatrix}
-\gamma_{13} & -\gamma_{13} & -\gamma_{13} & \Theta_{1c}^* & \Theta_{1c} & 0 & 0 & 0 & 0 & 0 & 0 & 0 & 0 & 0 & 0\\
-\gamma_{23} & -\gamma_{23} & -\gamma_{23} & 0 & 0 & \Theta_{2c}^* & \Theta_{2c} & 0 & 0 & 0 & 0 & 0 & 0 & 0 & 0\\
-\gamma_{03} & -\gamma_{03} & -\gamma_{03} & 0 & 0 & 0 & 0 & \Phi_{0c}^* & \Phi_{0c} & 0 & 0 & 0 & 0 & 0 & 0\\
-2\Theta_{1c} & -\Theta_{1c} & -\Theta_{1c} & p_{31} & 0 & 0 & 0 & 0 & 0 & -\Phi_{0c} & 0 & 0 & 0 & -\Theta_{2c} & 0\\
-2\Theta_{1c}^* & -\Theta_{1c}^* & -\Theta_{1c}^* & 0 & p_{31}^* & 0 & 0 & 0 & 0 & 0 & -\Phi_{0c}^* & 0 & 0 & 0 & -\Theta_{2c}^*\\
-\Theta_{2c} & -2\Theta_{2c} & -\Theta_{2c} & 0 & 0 & p_{32} & 0 & 0 & 0 & 0 & 0 & 0 & -\Phi_{0c} & 0 & -\Theta_{1c}\\
-\Theta_{2c}^* & -2\Theta_{2c}^* & -\Theta_{2c}^* & 0 & 0 & 0 & p_{32}^* & 0 & 0 & 0 & 0 & -\Phi_{0c}^* & 0 & -\Theta_{1c}^* & 0\\
-\Phi_{0c} & -\Phi_{0c} & -2\Phi_{0c} & 0 & 0 & 0 & 0 & p_{30} & 0 & 0 & -\Theta_{1c} & -\Theta_{2c} & 0 & 0 & 0\\
-\Phi_{0c}^* & -\Phi_{0c}^* & -2\Phi_{0c}^* & 0 & 0 & 0 & 0 & 0 & p_{30}^* & -\Theta_{1c}^* & 0 & 0 & -\Theta_{2c}^* & 0 & 0\\
0 & 0 & 0 & \Phi_{0c}^* & 0 & 0 & 0 & 0 & \Theta_{1c} & p_{01} & 0 & 0 & 0 & 0 & 0\\
0 & 0 & 0 & 0 & \Phi_{0c} & 0 & 0 & \Theta_{1c}^* & 0 & 0 & p_{01}^* & 0 & 0 & 0 & 0\\
0 & 0 & 0 & 0 & 0 & 0 & \Phi_{0c} & \Theta_{2c}^* & 0 & 0 & 0 & p_{20} & 0 & 0 & 0\\
0 & 0 & 0 & 0 & 0 & \Phi_{0c}^* & 0 & 0 & \Theta_{2c} & 0 & 0 & 0 & p_{20}^* & 0 & 0\\
0 & 0 & 0 & \Theta_{2c}^* & 0 & 0 & \Theta_{1c} & 0 & 0 & 0 & 0 & 0 & 0 & p_{21} & 0\\
0 & 0 & 0 & 0 & \Theta_{2c} & \Theta_{1c}^* & 0 & 0 & 0 & 0 & 0 & 0 & 0 & 0 & p_{21}^*
\end{bmatrix},
\tag{A4}
$$

$$
X_0 = \left[\tilde{\rho}_{11}^{(0)}\ \tilde{\rho}_{22}^{(0)}\ \tilde{\rho}_{00}^{(0)}\ \tilde{\rho}_{31}^{(0)}\ \tilde{\rho}_{13}^{(0)}\ \tilde{\rho}_{32}^{(0)}\ \tilde{\rho}_{23}^{(0)}\ \tilde{\rho}_{30}^{(0)}\ \tilde{\rho}_{03}^{(0)}\ \tilde{\rho}_{01}^{(0)}\ \tilde{\rho}_{10}^{(0)}\ \tilde{\rho}_{20}^{(0)}\ \tilde{\rho}_{02}^{(0)}\ \tilde{\rho}_{21}^{(0)}\ \tilde{\rho}_{12}^{(0)}\right]^T, \tag{A5}
$$

$$
B_0 = [-\gamma_{13}\ -\gamma_{23}\ -\gamma_{03}\ \Theta_{1c}\ -\Theta_{1c}^*\ \Theta_{2c}\ -\Theta_{2c}^*\ \Phi_{0c}\ -\Phi_{0c}^*\ 0\ 0\ 0\ 0\ 0\ 0]^T, \tag{A6}
$$

where $p_{31} = i(\Delta + \Delta_z) - \Gamma_{31}$, $p_{32} = i(\Delta - \Delta_z) - \Gamma_{32}$, $p_{30} = i\Delta - \Gamma_{30}$, $p_{01} = i\Delta_z - \Gamma_{01}$, $p_{20} = -i\Delta_z - \Gamma_{20}$, $p_{21} = -2i\Delta_z - \Gamma_{21}$, $\Theta_{1c} = -iG_1$, $\Theta_{2c} = -iG_2$, $\Phi_{0c} = -iG_0$, and T denotes the transpose of the vector.

$$A_{\pm} = \begin{bmatrix}
p'_{11} & -\gamma_{13} & -\gamma_{13} & \Theta^*_{1c} & \Theta_{1c} & 0 & 0 & 0 & 0 & 0 & 0 & 0 & 0 & 0 & 0 \\
-\gamma_{23} & p'_{22} & -\gamma_{23} & 0 & 0 & \Theta^*_{2c} & \Theta_{2c} & 0 & 0 & 0 & 0 & 0 & 0 & 0 & 0 \\
-\gamma_{03} & -\gamma_{03} & p'_{00} & 0 & 0 & 0 & 0 & \Phi^*_{0c} & \Phi_{0c} & 0 & 0 & 0 & 0 & 0 & 0 \\
-2\Theta_{1c} & -\Theta_{1c} & -\Theta_{1c} & p'_{31} & 0 & 0 & 0 & 0 & 0 & -\Phi_{0c} & 0 & 0 & 0 & -\Theta_{2c} & 0 \\
-2\Theta^*_{1c} & -\Theta^*_{1c} & -\Theta^*_{1c} & 0 & p'_{13} & 0 & 0 & 0 & 0 & 0 & -\Phi^*_{0c} & 0 & 0 & 0 & -\Theta^*_{2c} \\
-\Theta_{2c} & -2\Theta_{2c} & -\Theta_{2c} & 0 & 0 & p'_{32} & 0 & 0 & 0 & 0 & 0 & -\Phi_{0c} & 0 & -\Theta_{1c} & \\
-\Theta^*_{2c} & -2\Theta^*_{2c} & -\Theta^*_{2c} & 0 & 0 & 0 & p'_{23} & 0 & 0 & 0 & 0 & -\Phi^*_{0c} & 0 & -\Theta^*_{1c} & 0 \\
-\Phi_{0c} & -\Phi_{0c} & -2\Phi_{0c} & 0 & 0 & 0 & 0 & p'_{30} & 0 & 0 & -\Theta_{1c} & -\Theta_{2c} & 0 & 0 & 0 \\
-\Phi^*_{0c} & -\Phi^*_{0c} & -2\Phi^*_{0c} & 0 & 0 & 0 & 0 & 0 & p'_{03} & -\Theta^*_{1c} & 0 & 0 & -\Theta^*_{2c} & 0 & 0 \\
0 & 0 & 0 & \Phi^*_{0c} & 0 & 0 & 0 & 0 & \Theta_{1c} & p'_{01} & 0 & 0 & 0 & 0 & 0 \\
0 & 0 & 0 & 0 & \Phi_{0c} & 0 & 0 & \Theta^*_{1c} & 0 & 0 & p'_{10} & 0 & 0 & 0 & 0 \\
0 & 0 & 0 & 0 & 0 & 0 & \Phi_{0c} & \Theta^*_{2c} & 0 & 0 & 0 & p'_{20} & 0 & 0 & 0 \\
0 & 0 & 0 & 0 & 0 & \Phi^*_{0c} & 0 & 0 & \Theta_{2c} & 0 & 0 & 0 & p'_{02} & 0 & 0 \\
0 & 0 & 0 & \Theta^*_{2c} & 0 & 0 & \Theta_{1c} & 0 & 0 & 0 & 0 & 0 & 0 & p'_{21} & 0 \\
0 & 0 & 0 & 0 & \Theta_{2c} & \Theta^*_{1c} & 0 & 0 & 0 & 0 & 0 & 0 & 0 & 0 & p'_{12}
\end{bmatrix}, \tag{A7}$$

$$X_{\pm} = \left[\tilde{\rho}'^{(\pm1)}_{11}\ \tilde{\rho}'^{(\pm1)}_{22}\ \tilde{\rho}'^{(\pm1)}_{00}\ \tilde{\rho}'^{(\pm1)}_{31}\ \tilde{\rho}'^{(\pm1)}_{13}\ \tilde{\rho}'^{(\pm1)}_{32}\ \tilde{\rho}'^{(\pm1)}_{23}\ \tilde{\rho}'^{(\pm1)}_{30}\ \tilde{\rho}'^{(\pm1)}_{03}\ \tilde{\rho}'^{(\pm1)}_{01}\ \tilde{\rho}'^{(\pm1)}_{10}\ \tilde{\rho}'^{(\pm1)}_{20}\ \tilde{\rho}'^{(\pm1)}_{02}\ \tilde{\rho}'^{(\pm1)}_{21}\ \tilde{\rho}'^{(\pm1)}_{12}\right]^T, \tag{A8}$$

$$B_+ = \left[\frac{i}{\sqrt{2}}\tilde{\rho}^{(0)}_{13}\ 0\ 0\ -\frac{i}{\sqrt{2}}\left(2\tilde{\rho}^{(0)}_{11} + \tilde{\rho}^{(0)}_{22} + \tilde{\rho}^{(0)}_{00} - 1\right)\ 0\ -\frac{i}{\sqrt{2}}\tilde{\rho}^{(0)}_{12}\ 0\ -\frac{i}{\sqrt{2}}\tilde{\rho}^{(0)}_{10}\ 0\ \frac{i}{\sqrt{2}}\tilde{\rho}^{(0)}_{03}\ 0\ 0\ 0\ \frac{i}{\sqrt{2}}\tilde{\rho}^{(0)}_{23}\ 0\right]^T, \tag{A9}$$

$$B_- = \left[0\ \frac{i}{\sqrt{2}}\tilde{\rho}^{(0)}_{23}\ 0\ -\frac{i}{\sqrt{2}}\tilde{\rho}^{(0)}_{21}\ 0\ -\frac{i}{\sqrt{2}}\left(\tilde{\rho}^{(0)}_{11} + 2\tilde{\rho}^{(0)}_{22} + \tilde{\rho}^{(0)}_{00} - 1\right)\ 0\ -\frac{i}{\sqrt{2}}\tilde{\rho}^{(0)}_{20}\ 0\ 0\ 0\ 0\ \frac{i}{\sqrt{2}}\tilde{\rho}^{(0)}_{03}\ 0\ \frac{i}{\sqrt{2}}\tilde{\rho}^{(0)}_{13}\right]^T, \tag{A10}$$

where $p'_{11} = i\omega_{pc} - \gamma_{13}$, $p'_{22} = i\omega_{pc} - \gamma_{23}$, $p'_{00} = i\omega_{pc} - \gamma_{03}$, $p'_{31} = i(\omega_{pc} + \Delta + \Delta_z) - \Gamma_{31}$, $p'_{13} = -i(-\omega_{pc} + \Delta + \Delta_z) - \Gamma_{31}$, $p'_{32} = i(\omega_{pc} + \Delta - \Delta_z) - \Gamma_{32}$, $p'_{23} = -i(-\omega_{pc} + \Delta - \Delta_z) - \Gamma_{32}$, $p'_{30} = i(\omega_{pc} + \Delta) - \Gamma_{30}$, $p'_{03} = -i(-\omega_{pc} + \Delta) - \Gamma_{30}$, $p'_{01} = i(\omega_{pc} + \Delta_z) - \Gamma_{01}$, $p'_{10} = i(\omega_{pc} - \Delta_z) - \Gamma_{01}$, $p'_{20} = i(\omega_{pc} - \Delta_z) - \Gamma_{20}$, $p'_{02} = i(\omega_{pc} + \Delta_z) - \Gamma_{20}$, $p'_{21} = i(\omega_{pc} - 2\Delta_z) - \Gamma_{21}$, and $p'_{12} = i(\omega_{pc} + 2\Delta_z) - \Gamma_{21}$. The first three elements of the column vector X_0 provide the population of the atomic levels. The first-order coherence terms $\tilde{\rho}^{(+1)}_{31}$ and $\tilde{\rho}^{(-1)}_{32}$ can be obtained from X_+ and X_-, respectively.

[1] I. Cindrich, Image scanning by rotation of a hologram, Appl. Opt. **6**, 1531 (1967).

[2] W. B. Jackson, N. M. Amer, A. C. Boccara, and D. Fournier, Photothermal deflection spectroscopy and detection, Appl. Opt. **20**, 1333 (1981).

[3] R. W. Dixon, Photoelastic properties of selected materials and their relevance for applications to acoustic light modulators and scanners, J. Appl. Phys. **38**, 5149 (1967).

[4] T. C. Lee and J. D. Zook, Light beam deflection with electrooptic prisms, IEEE J. Quantum Electron. **4**, 442 (1968).

[5] G. P. Agarwal, Induced Focusing of Optical Beams in Self-Defocusing Nonlinear Media, Phys. Rev. Lett. **64**, 2487 (1990).

[6] R. R. Moseley, S. Shepherd, D. J. Fulton, B. D. Sinclair, and M. H. Dunn, Spatial Consequences of Electromagnetically Induced Transparency: Observation of Electromagnetically Induced Focusing, Phys. Rev. Lett. **74**, 670 (1995).

[7] R. R. Moseley, S. Shepherd, D. J. Fulton, B. D. Sinclair, and M. H. Dunn, Electromagnetically-induced focusing, Phys. Rev. A **53**, 408 (1996).

[8] R. Kapoor and G. S. Agarwal, Theory of electromagnetically induced waveguides, Phys. Rev. A **61**, 053818 (2000).

[9] D. Bortman-Arbiv, A. D. Wilson-Gordon, and H. Friedmann, Strong parametric amplification by spatial soliton-induced cloning of transverse beam profiles in an all-optical antiwaveguide, Phys. Rev. A **63**, 031801(R) (2001).

[10] R. Schlesser and A. Weis, Light-beam deflection by cesium vapor in a transverse-magnetic field, Opt. Lett. **17**, 1015 (1992).

[11] R. Holzner, P. Eschle, S. Dangel, R. Richard, H. Schmid, U. Rusch, B. Rohricht, R. J. Ballagh, A. W. McCord, and W. J. Sandle, Observation of Magnetic-Field-Induced Laser Beam Deflection in Sodium Vapor, Phys. Rev. Lett. **78**, 3451 (1997).

[12] L. Karpa and M. Weitz, A Stern-Gerlach experiment for slow light, Nat. Phys. **2**, 332 (2006).

[13] V. A. Sautenkov, H. Li, Y. V. Rostovtsev, and M. O. Scully, Ultradispersive adaptive prism based on a coherently prepared atomic medium, Phys. Rev. A **81**, 063824 (2010).

[14] Q. Sun, Y. V. Rostovtsev, and M. S. Zubairy, Optical beam steering based on electromagnetically induced transparency, Phys. Rev. A **74**, 033819 (2006).

[15] D. L. Zhou, L. Zhou, R. Q. Wang, S. Yi, and C. P. Sun, Deflection of slow light by magneto-optically controlled atomic media, Phys. Rev. A **76**, 055801 (2007).

[16] H. R. Zhang, L. Zhou, and C. P. Sun, Birefringence lens effects of an atom ensemble enhanced by an electromagnetically induced transparency, Phys. Rev. A **80**, 013812 (2009).

[17] L. Zhou, J. Lu, D. L. Zhou, and C. P. Sun, Quantum theory for spatial motion of polaritons in inhomogeneous fields, Phys. Rev. A **77**, 023816 (2008).

[18] C. Hang and G. Huang, Stern-Gerlach effect of weak-light ultraslow vector solitons, Phys. Rev. A **86**, 043809 (2012).

[19] C. Zhu, L. Dang, and E. W. Hagley, Dynamic light deflection in an active Raman-gain medium using a spatially inhomogeneous pump, Phys. Rev. A **88**, 013841 (2013).

[20] O. N. Verma and T. N. Dey, Steering, splitting, and cloning of an optical beam in a coherently driven Raman gain system, Phys. Rev. A **91**, 013820 (2015).

[21] O. Hoston and P. Kwait, Observation of the spin Hall effect of light via weak measurements, Science **319**, 787 (2008).

[22] P. B. Dixon, D. J. Starling, A. N. Jordan, and J. C. Howell, Ultrasensitive Beam Deflection Measurement Via Interferometric Weak Value Amplification, Phys. Rev. Lett. **102**, 173601 (2009).

[23] Y. Aharonov, D. Z. Albert, and L. Vaidman, How the Result of a Measurement of a Component of the Spin of a Spin-1/2 Particle can Turn out to be 100, Phys. Rev. Lett. **60**, 1351 (1988).

[24] N. Brunner, A. Acin, D. Collins, N. Gisin, and V. Scarani, Optical Telecom Networks as Weak Quantum Measurements with Postselection, Phys. Rev. Lett. **91**, 180402 (2003).

[25] P. Kumar and S. Dasgupta, Estimation of temporal separation of slow light pulses in atomic vapors by weak measurement, Phys. Rev. A **91**, 043803 (2015).

[26] A. Ghosh and P. Fischer, Chiral Molecules Split Light: Reflection and Refraction in a Chiral Liquid, Phys. Rev. Lett. **97**, 173002 (2006).

[27] E. U. Condon, Theories of optical rotatory power, Rev. Mod. Phys. **9**, 432 (1937).

[28] Y. Guo, L. Zhou, L. M. Kuang, and C. P. Sun, Magneto-optical Stern-Gerlach effect in an atomic ensemble, Phys. Rev. A **78**, 013833 (2008).

[29] L. Allen, M. W. Beijersbergen, R. J. C. Spreeuw, and J. P. Woerdman, Orbital angular momentum of light and the transformation of Laguerre-Gaussian laser modes, Phys. Rev. A **45**, 8185 (1992).

[30] S. Kumar, T. Lauprêtre, F. Bretenaker, F. Goldfarb, and R. Ghosh, Polarization-dependent manipulation of optical properties in a tripod system, Phys. Rev. A **88**, 023852 (2013).

[31] D. Steck, Alkali D line data, http://steck.us/alkalidata/.

[32] G. S. Agrawal and S. Dasgupta, Coherent medium as a polarization splitter of pulses, Phys. Rev. A **65**, 053811 (2002).

[33] S. F. Arnold, M. Arndt, and A. Zeilinger, Magneto-optical effects with cold lithium atoms, J. Phys. B **34**, 2527 (2001).

[34] B. S. Ham and P. R. Hemmer, Coherent Switching in a Four-Level System: Quantum Switching, Phys. Rev. Lett. **84**, 4080 (2000).

[35] M. Born and E. Wolf, *Principles of Optics* (Cambridge University Press, Cambridge, 1999).

[36] Q. Sun, Y. V. Rostovtsev, J. P. Dowling, M. O. Scully, and M. S. Zubairy, Optical controlled delays for broadband pulses, Phys. Rev. A **72**, 031802(R) (2005).

[37] A. G. Truscott, M. E. J. Friese, N. R. Heckenberg, and H. Rubinsztein-Dunlop, Optical Written Waveguide in an Atomic Vapor, Phys. Rev. Lett. **82**, 1438 (1999).